Electrochimica Acta 462 (2023) 142746

Contents lists available at ScienceDirect

Electrochimica Acta

journal homepage: www.journals.elsevier.com/electrochimica-acta

Sustainable lithium-ion battery separators based on cellulose and soy protein membranes

João P. Serra [a,b], Jone Uranga [c], Renato Gonçalves [d], Carlos M. Costa [a,b,e,*], Koro de la Caba [c,f], Pedro Guerrero [c,f,*], Senentxu Lanceros-Mendez [a,b,f,g]

[a] Physics Centre of Minho and Porto Universities (CF-UM-UP), University of Minho, Braga 4710-057, Portugal
[b] Laboratory of Physics for Materials and Emergent Technologies, LapMET, University of Minho, Braga 4710-057, Portugal
[c] BIOMAT Research Group, University of the Basque Country (UPV/EHU), Escuela de Ingeniería de Gipuzkoa, Plaza de Europa 1, 20018, Donostia-San Sebastián, Spain
[d] Centre of Chemistry, University of Minho, Braga 4710-057, Portugal
[e] Institute of Science and Innovation for Bio-Sustainability (IB-S), University of Minho, Braga 4710-057, Portugal
[f] BCMaterials, Basque Center for Materials, Applications and Nanostructures, UPV/EHU Science Park, Leioa 48940, Spain
[g] Ikerbasque, Basque Foundation for Science, Bilbao 48009, Spain

ARTICLE INFO

Keywords:
Soy protein
Cellulose
Membrane
Separator
Lithium-ion batteries

ABSTRACT

The food industry produces millions of tons of natural by-products. Through this study, we followed an environmentally friendly strategy using discards, such as soy protein isolate (SPI) from soya oil production and marine cellulose (Cell) from the agar industry, in order to achieve added-value applications. In particular, this work focuses on the development of membranes based on soy protein and cellulose, and their validation as battery separator membranes toward sustainable energy storage systems. SPI membranes with Cell show excellent compatibility with the electrolyte based on physical interactions. These physical interactions favor the swelling of the membranes, reaching swelling values of 1000% after three days in the liquid electrolyte. The membranes are thermally stable up to 180 °C. After being subjected to the liquid electrolyte, it is observed that the microstructure of the membranes change, but the porous structure is maintained, while the materials remain easy to handle. The ionic conductivity value, lithium transference number and battery performance in cathodic half-cells are ~ 5.8 mS.cm^{-1}, 0.77, and 112 mAh.g^{-1} at 1C-rate, respectively. Overall, considering environmental issues and circular economy, it is proven that it is possible to obtain more sustainable high-performance lithium-ion batteries based on waste materials.

1. Introduction

Energy has been intrinsically linked to human activities over the years. Excluding energy from food that humans need for their metabolism, the first major advance in the use of energy to benefit human activities took place in the Paleolithic, with the use of fire from burning wood to heat and cook some foods and in the Neolithic with the use of wood burning fire to shape metallurgical tools [1]. In the 18th century, in England, coal began to be used as a substitute for wood, since its use was more efficient. This discovery was applied to industry, witnessing the implementation of coal-powered systems, leading to the first industrial revolution at the end of the same century [2]. At the beginning of the 20th century, in the United States, petroleum began to be used as one of the forms of energy production. All these discoveries were important for the development of human activities and to reach the quality of life that we currently have, allowing also for an exponential population growth up to the more than 8 billion people in the world we are nowadays [3].

At the end of the 20th century, it was realized that fossil fuels were finite and that at the level at which they were being used they could become scarce or even run out. It began to be realized that energy could be a big problem in the world, since the energy costs of current human quality of life are high, the number of people in the world is constantly increasing, together with the environmental impact of human activities. Thus, new concerns such as climate change and global warming emerged, being felt all over the world. It was realized that systems powered by fossil fuels brought negative consequences for the planet and for the sustainability of future generations [4]. One of the

* Corresponding authors.
E-mail addresses: cmscosta@fisica.uminho.pt (C.M. Costa), pedromanuel.guerrero@ehu.es (P. Guerrero).

https://doi.org/10.1016/j.electacta.2023.142746
Received 19 May 2023; Received in revised form 14 June 2023; Accepted 15 June 2023
Available online 16 June 2023

alternatives to these polluting energy sources appears at the end of the 20th century with the implementation of systems capable of generating energy through renewable sources, this means, systems that use sunlight (photovoltaics), wind, water (dams, wave and tidal energy) and nuclear energy systems. Several of these systems have the great advantage of not polluting during power generation but have some limitations such as intermittency and the need to have specific favorable conditions for power generation [5,6]. The solutions for the intermittence of renewable energies include the development of hybrid systems, including both renewable and non-renewable sources, and/or the development of renewable energy generation systems coupled with energy storage systems, allowing the storage of excess energy generated to be used in case of unfavorable conditions in the production of energy by the same source [7,8]. Batteries thus play an essential role in this type of systems. Further, batteries are nowadays heavily used in portable and small devices such as mobile phones, computers or tablets and in larger devices such as electric cars and autonomous energy systems [9].

Batteries are electrochemical systems based on oxidation-reduction reactions that convert chemical energy into electrical energy and vice versa. Batteries are made up of two electrodes (cathode and anode) and a separator soaked in an electrolyte solution [10]. Over the last few years, batteries have undergone changes according to needs and according to the applications in which they are implemented. Currently, the most commercialized batteries are lithium-ion batteries (LIBs) due to their high energy density, long life cycles and low weight and size when compared to other types of batteries [11]. Nevertheless, batteries are composed by materials that, from an environmental point of view, could translate into future problems. Sustainability in batteries can be complex, but it starts with replacing some of these materials by sustainable ones [12]. Sustainable materials are those with the friendliest extraction process, production, use, lifetime and recycling so that they do not put at risk future generations [13].

Natural polymers are called to play an essential role in this new generation of sustainable materials, since they are naturally obtained from animals or plants, are renewable sources and their degradation at the end of life occurs naturally and faster compared to synthetic polymers [14]. Some of these types of polymers are already starting to be used as battery separators, such as carrageenan [15], cellulose [16], cellulose succinate nanofibers (SCNF) [17], poly (hydroxybutyrate-co-hydroxyvalerate) (PHBV) [18], poly(L-lactic acid) (PLLA) [19] and silk [20], with promising results. Biomass derived separators are particularly relevant, since they are abundant, are compatible with simple/cheap processing methods and their use is in line with circular economy and sustainable development policy guidelines [21]. Among biomass-derived separators, cellulose is widely used, inasmuch as it presents wide availability and superior features in the fields of electrolyte uptake capability, mechanical strength and thermal/chemical stability [22]. In fact, a commercial cellulose-based separator has already been produced for lithium secondary batteries [23] and also tested with NCM523 ($LiNi_{0.5}Co_{0.2}Mn_{0.3}O_2$) cathodes with ionic conductivity value of 6.34 $mS.cm^{-1}$ and lithium ion transference number value of 0.82 at room temperature [24]. However, pretreatment, separation, and functionalization of cellulose sometimes can be complex, and harmful byproducts can be generated. In this sense, unlike cellulose derived from plants, cellulose derived from algae is free of lignin, which facilitates cellulose extraction [25]. It is worth highlighting that this algae cellulose can be obtained from agar production waste valorization [26]. Therefore, algae cellulose use in batteries will lead to cheaper and more environmentally friendly separators.

Within the various sustainable materials, soy protein can also be seen as an alternative to conventional synthetic polymers used in LIB. Soy protein has the advantages of being sustainable, environmentally friendly, renewable and degradable. Soy protein is extracted from beans and is marketed in three types: soy flour, soy protein concentrate, and soy protein isolate (SPI) [27]. SPI can be used as films, plastics, coatings, adhesives, emulsifiers and hydrogels [28]. Due to these various ways of processing, SPI is widely used in some particular industries such as food supplements and animal feed, but it can also be used in some specific applications such as biomedical materials, tissue engineering and sensors [29,30]. Despite its environmentally friendly characteristics, SPI tends to have a certain rigidity, which limits its use in some applications that need to be mechanically flexible, shows low mechanical strength and low water resistance properties [31]. The solution for solving the mechanical problems presented by soy protein involves the use of this sustainable material with the use of a filler. Cellulose, in addition of being a sustainable filler and with the same environmental advantages as soy protein, has excellent mechanical strength and a high aspect ratio, providing soy protein with the required characteristics to be used as a LIBs separator [32]. Further, it is to notice that both soy protein and cellulose are obtained from food industry discards, contributing therefore to a waste limited and sustainable economy through the revalorization of waste to high end applications. Similar to cellulose, proteins show attractive advantages for fabricating separators. Together with hierarchical structures and specific biophysical/biochemical properties, proteins have abundant polar groups, useful for creating strong interactions with lithium ions [33]. A protein with enormous studies in different fields, like SPI, still needs in-depth research in the scope of energy storage systems.

In this context, the objective of this work is to develop LIB separators based on natural materials for a new generation of sustainable batteries. Separators based on SPI with different amounts of cellulose were developed through a freeze-drying process, and the influence of filler content on separator membranes was evaluated through their morphological, crystallographic, thermal, physicochemical and mechanical properties. The developed membranes were also tested for battery applications by assessing electrolyte uptake, ionic conductivity and lithium transfer number, as well as charge-discharge half-cell battery tests. Furthermore, the valorization of biomass or by-products from industry, rich on proteins and polysaccharides, can be a worthy approach to prepare sustainable battery components. Taking all this into account, this work focusses on the evaluation of soy protein/algae cellulose membranes as battery separator in order to contribute to the design of next-generation sustainable green separators.

2. Experimental details

2.1. Materials

Soy protein isolate (SPI), PROFAM 974, with a 90% protein content on dry basis, was obtained from ADM Protein Specialties Division (Netherlands). Glycerol, used as plasticizer, and NaOH (1 M) were supplied by Panreac (Spain). The algae waste was generated from the processing of the red algae *Gelidium* (*Rodophyta*) to obtain agar and it was kindly provided by Roko Industries S.A. (Llanera, Asturias Spain). This algae waste is mainly composed of cellulose and protein.

The N-methylpyrrolidinone (NMP) solvent, lithium-metallic and electrolyte solution of 1 M $LiPF_6$ in a mixture of dimethyl carbonate (DMC) and ethyl carbonate (EC) (1:1 in vol. ratio) were purchased by Merck. C-$LiFePO_4$ (LFP), super P carbon black, and poly(vinylidene fluoride) PVDF, Kynar PVDF HSV900, were acquired by Phostech Lithium, Timcal Graphite & Carbon and, Arkema, respectively.

2.2. Processing of membranes

SPI and algae cellulose-containing membranes were prepared by lyophilisation. First, 10 g of SPI was mixed with 0, 25, 30, 30, 40 and 50 wt% of algae residues (SPI dry basis) and 125 mL of distilled water were added. The mixture was then heated at 80 °C for 30 min under magnetic stirring. Then, 30 wt % glycerol (SPI dry basis) was added to the mixture and the pH was adjusted to 10 with NaOH (1 M) and the mixture was heated for another 30 min under the same conditions to obtain a homogeneous mixture. Finally, the mixture was poured into molds, kept in

a freezer at -23 °C for 48 h and then, freeze-dried for 72 h to obtain the membranes. The cellulose-containing algae waste (Cell) amounts employed in this work were 0, 25, 30, 40 and 50 wt % (based on SPI dry basis). The membranes were identified as control in case of the sample without algae waste and 25Cell, 30Cell, 40Cell and 50Cell as a function of cellulose-containing algae waste amount.

2.3. Physicochemical characterization of membranes

The morphology of the samples was visualized using an S-4800 field emission scanning electron microscope (Hitachi High-Technologies Corporation). Samples were mounted on a metal stub with a double-side adhesive tape and coated under vacuum with gold (JFC-1100) in an argon atmosphere prior to observation. Membranes were measured using an accelerating voltage of 5 kV. Furthermore, scanning electron microscopy (SEM) images were analyzed by ImageJ software for pore size evaluation and the porosity was quantified by PoreMaster GT-60 Mercury-intrusion apparatus (Quantachrome Instruments), equipped with low-pressure (0.1 psi) and high-pressure (60000 psi) devices. Before testing, membranes were dried at 105 °C for 12 h and then, the density was measured in an automatic He Microultra Pycnometer (Quantachrome Instruments).

Rectangular pieces of 2 × 2 cm were weighed (w_i), and then immersed into lithium-salt electrolyte solution. Samples were weighed after immersion for specific times (w_t) until constant values were obtained. The electrolyte uptake (ELU) was calculated by the following equation:

$$ELU(\%) = \frac{w_t - w_i}{w_i} \cdot 100 \quad (1)$$

Fourier transform infrared (FTIR) spectroscopy was carried out in the membranes before and after electrolyte uptake tests on a Platinum-ATR Alpha II FTIR spectrometer (Bruker). A total of 32 scans were performed at a resolution of 4 cm^{-1} in the wavenumber range from 800 to 4000 cm^{-1}.

X-ray diffraction (XRD) analysis was carried out using a diffraction unit (PANalyticXpert PRO) operating at 40 kV and 40 mA. The radiation was generated from a Cu-Kα (λ = 1.5418 Å) source. Data were collected at 2θ values from 2 to 50°, where θ is the incidence angle of the X-ray beam on the sample.

Thermo-gravimetric analysis (TGA) was performed in a Mettler Toledo TGA SDTA 851 equipment (Mettler Toledo S.A.E.). Samples were heated from 25 to 800 °C at a heating rate of 10 °C/min under inert atmosphere conditions (10 mL N_2/min) to avoid thermo-oxidative reactions.

Differential scanning calorimetry (DSC) was carried out in a Mettler Toledo DSC 822 (Mettler Toledo S.A.E.). Samples (3.0 ± 0.2 mg) were sealed in an aluminum pan to avoid mass loss during the experiment. Filled pans were heated from -50 to 300 °C at a rate of 10 °C/min under inert atmosphere conditions (10 mL N_2/min) to avoid thermo-oxidative reactions.

Mechanical properties were performed employing a TA.XT.Plus C Texture Analyzer (Aname Instrumentación Científica). For compression tests, assays were carried out up to 50% deformation with a 50 kg load cell, and data were collected at 1 mm/s speed. For puncture tests, a 5 kg load cell was employed and data were collected at 3 mm/s speed. Additionally, texture profile analysis (TPA) was carried out up to 20% deformation, using the 50 kg load cell, and data were collected at 1 mm/s speed.

2.4. Electrochemical parameters of membranes

For the determination of the ionic conductivity value, electrochemical impedance spectroscopy was used through symmetric cells with stainless steel disc electrodes. The separator sample, with thickness of approx. 100 μm, was embedded with the electrolyte, placed between the electrodes and pretreated at 60 °C in a Buchi tube. The measurements were performed with a Biologic VMP3 instrument in the frequency range from 0.1 mHz to 106 Hz and an amplitude of 10 mV at room temperature. The ionic conductivity (σ_i) value was obtained through the following equation:

$$\sigma_i = \frac{d}{R_b \times A} \quad (2)$$

where d is the thickness of the separator sample, R_b is the bulk resistance and A is the electrode area.

Regarding to the electrochemical stability window, room temperature cyclic voltammetry was used through a two-electrode cell configuration composed with a 25 μm diameter gold microelectrode and lithium metal. Measurements were carried out at room temperature with a Biologic VMP3 instrument at 0.1 mV/s inside a dry argon-filled glovebox.

The Li-ion transference number (t^+_{Li}) was determined using symmetrical lithium cells through the potentiostatic polarization and applying a DC voltage of 10 mV at room temperature [34]. The t^+_{Li} value was determined by applying Eq. 3:

$$t_{Li^+} = \frac{I^s\left[\Delta V - I^0 R^0\right]}{I^0\left[\Delta V - I^s R^s\right]} \quad (3)$$

where I_s and I_0 are the steady and initial currents, respectively, ΔV is the applied potential, and R^0 and R^s are the initial and final resistances of the Li electrode/electrolyte before and after polarization, respectively.

2.5. Battery preparation, assembly and characterization

The cathodic half-cells were assembled with lithium metal |SPE| LFP cathode configuration in a glovebox under argon atmosphere (H_2O, O_2 < 1 ppm). Prior to assembly, the LFP cathode material and the separator membrane were transferred to the glovebox, after being dried at 60 °C under vacuum overnight in a Buchi TO51 tube oven. LFP cathodes were prepared with an active material:conductive material:polymer binder composition in a weight ratio of 80:10:10 and deposited on an aluminum current collector with an active mass loading about 2 mg. More details on the preparation are explained in [35]. Galvanostatic charge-discharge cycles were carried out at room temperature in a Landt CT2001A instrument at different rates (C/10, C/5, C/2, 1C and 2C, C = 170 $mA.g^{-1}$) for 10 cycles and C/5 rate for 100 cycles. Before and after cycling, impedance spectroscopy was carried out in the batteries with a signal amplitude of 10 mV in the frequency range from 10 mHz to 500 kHz with a Solartron 1260A Impedance Analyzer instrument.

3. Results and discussion

3.1. Morphology, degree of porosity and pore size

The developed easy-to-handle membranes were obtained in a circular shape and with uniform distribution. As presented in Fig. 1, the appearance of the membranes is different between the control sample and the membranes with algae cellulose, due to the presence of algae cellulose. On the other hand, there are no relevant differences between membranes with different algae waste content.

The morphology of the developed membranes is shown in Fig. 2 through the SEM images. Regardless of the algae waste cellulose (Cell) content, Fig. 2a–d, it is observed that the membranes show a porous morphology with interconnected pores distributed throughout the sample, which is ascribed to the processing methodology. Moreover, it can be visualized that SPI and algae cellulose had good compatibility due to the uniform membrane appearance. After the uptake process with electrolyte solution, (Fig. 2e and f), and independently of Cell content, the porous morphology of the membranes is maintained, demonstrating the excellent stability of the membrane in the electrolyte solution. The

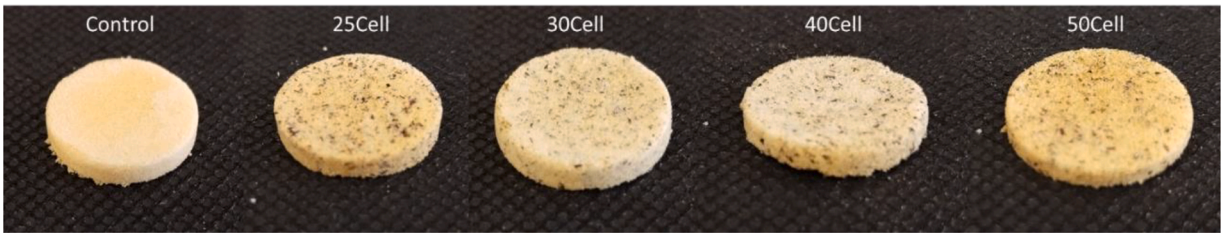

Fig. 1. Optical images of control, 25Cell, 30Cell, 40Cell and 50Cell membranes.

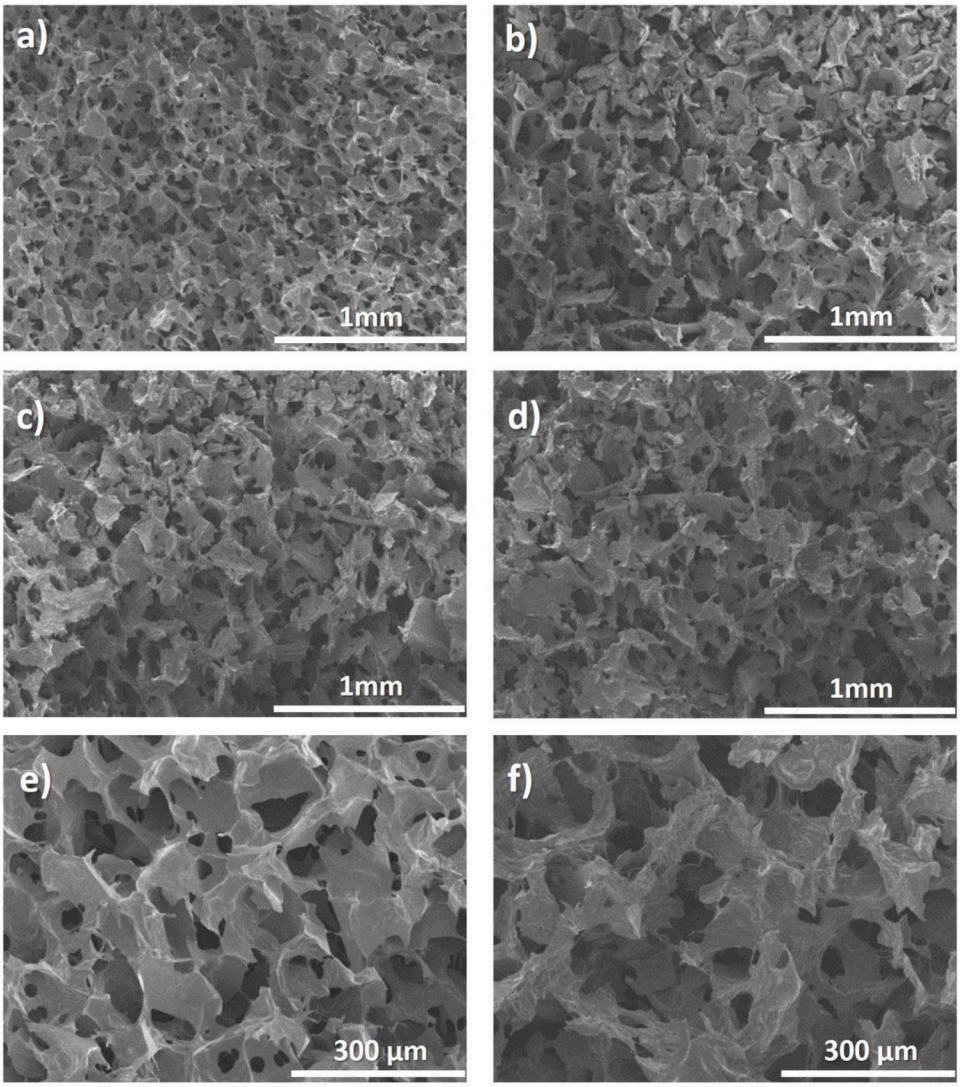

Fig. 2. Cross section morphology of the membranes: (a) Control, (b) 25Cell, (c) 40Cell and (d) 50Cell. Morphology after uptake process for (e) Control and (f) 50Cell.

degree of porosity of the membranes, as determined by mercury intrusion porosimetry (MIP), is in the order of 80–90%, regardless of alga waste content.

Fig. 3 shows the pore size for each membrane, the average pore size increasing with increasing Cell content. The main reason for this behavior is the microphase separation between polymers, decreasing SPI amount promoting aggregation and inhibiting the ordered re-assembly of cellulose molecular chains [36]. This intrinsic pore structure contributes to the excellent liquid electrolyte wettability [37]. Owing to the curvature of the pores and the interpenetrated microporous structure achieved, these membranes can effectively inhibit the occurrence of lithium dendrites on the graphite anode during the charge process, being more suitable for batteries with a long cycle life [38]. The control membrane porosity was 83% and slightly increased as the amount of algae waste cellulose increased, showing a porosity of 89% for 50Cell membranes.

3.2. *Physicochemical characterization*

The electrolyte wettability and uptake capacity of separators play a key role in their electrochemical performance. In this way, first, electrolyte contact angle was intended to be measured, but it was not possible since the electrolyte droplet was fully absorbed into the samples. However, these trials were useful to confirm that samples had

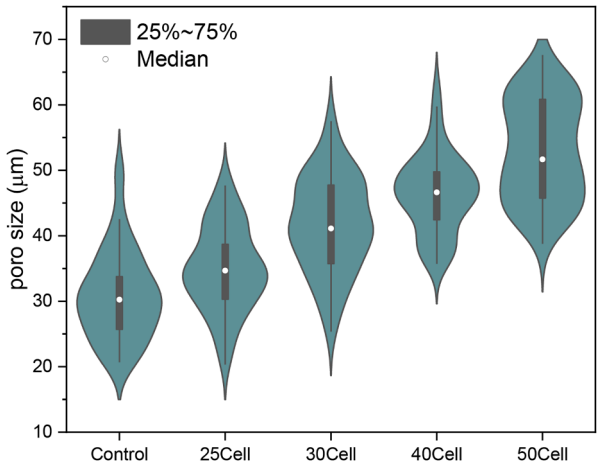

Fig. 3. Pore size for control, 25Cell, 30Cell, 40Cell and 50Cell membranes.

excellent liquid electrolyte wettability, as well as to prove that samples and electrolyte were affine, in as much as the lower the contact angle, the greater the affinity [39]. The electrolyte absorption capacity of the samples was investigated as a function of time. As presented in Fig. 4a, all samples had a prolonged electrolyte uptake, without any saturation plateau in the first 7 days. Control sample showed faster and higher electrolyte uptake values. These ELU values decreased as the algae cellulose content increased, but ELU value was around 1000% at the end of the test for 50Cell membranes. The obtained values are higher than those found for current commercial separators (~150%), mainly fabricated from PE and PP [40]. Also, it is observed that this process decreases with increasing the cell amount due to the morphologies with different pore size. As the pore size increases, the free void volume increases and consequently decreases the swelling process, since this process occurs in the amorphous phase of the membrane [41].

Regarding FTIR, spectra showed typical bands of SPI and cellulose (Fig. 4b). The major characteristic bands of SPI are amide I (around 1630 cm^{-1}) and amide II (around 1530 cm^{-1}) [42,43]. Cellulose shows characteristic bands related to β-(1→4)-linked glucan [44], such as the band around 1033 cm^{-1}. It is worth noting the absence of bands at 1413, 1533, and 1726 cm^{-1}, indicating the absence of lignin [45]. The addition of algae cellulose did not lead to new bands, therefore, no chemical reactions occurred between SPI and the cellulose present in algae waste [46] but physical interactions between amino and hydroxyl groups of SPI and hydroxyl groups of cellulose [42,47]. The abundance of hydroxyl groups, which are electrolyte-friendly groups, is the main reason for the excellent electrolyte wettability [37]. The electrolyte presence was clearly shown in the membrane spectra carried out after electrolyte uptake, which showed the characteristic electrolyte bands at ≈ 1800, 1760, 1160, 1070, and 840 cm^{-1} (Fig. 4b).

Control and algae cellulose-containing samples were analyzed by means of X-ray diffraction (XRD) to identify the membrane structure. Fig. 4c shows that all samples exhibited two broad peaks at 9° and 20°. The first peak was associated to the α-helix of SPI, while the second peak was attributed to the β-sheet structures of SPI, as well as to cellulose present in algae waste [48,49]. All samples had almost identical XRD patterns, thereby, the amorphous structure of SPI was maintained even when protein was blended with cellulose and physical interactions were formed between both polymers. XRD was also analyzed after electrolyte uptake (Fig. 4d). The two sharp peaks around 39 and 45° were associated to LiF. It is observed that the presence of the electrolyte caused some changes in the secondary structure of SPI. The peak around 9° disappeared owing to some inter-peptide hydrogen bonding modifications and the disappearance of the α-helix conformation. Moreover, control membrane showed more noticeable changes in the secondary structure with a decrease in the intensity of the peak located around 20°, while this peak showed similar intensity for the membranes with algae cellulose, indicating that these membranes maintained β-sheet structure.

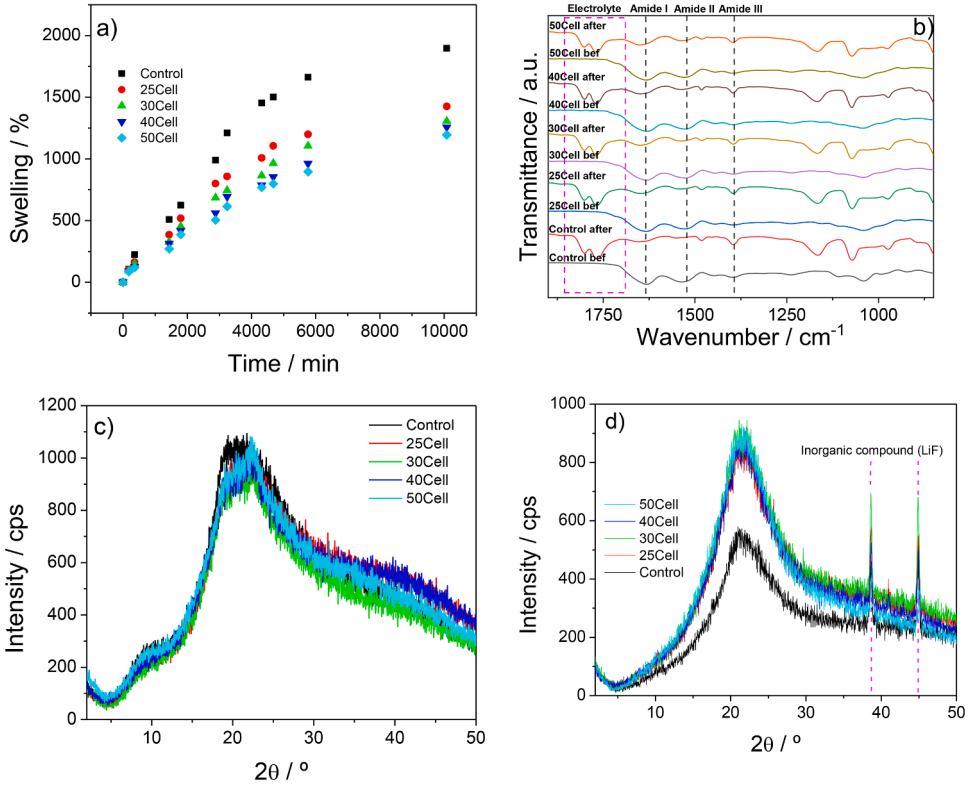

Fig. 4. (a) Swelling behavior, (b) FTIR spectra before and after electrolyte swelling, and XRD spectra (c) before and (d) after electrolyte swelling for control, 25Cell, 30Cell, 40Cell and 50Cell membranes.

Battery separators need thermal stability to avoid safety concerns [50]. In this sense, DSC and TGA analyses were carried out to assess the membrane thermal properties, as shown in Fig. 5a and b, respectively. Regarding DSC analysis, two peaks were found up to 300 °C, as presented in Fig. 5a. These peaks were ascribed to SPI and, specifically, to the denaturation of 7S (84–90 °C) and 11S (230–240 °C) globulins [46]. The denaturation peak associated to 11S globulins is typically observed at lower temperatures, but moisture content in membranes could shift its position to higher temperatures [51,52]. Regarding TGA, derivative thermo-gravimetric (DTG) curves and weight loss curves are shown in Fig. 5b. Three main stages of thermal degradation are observed. The first stage around 100 °C is related to the evaporation of the water present in the structure, the second weight loss around 200 °C is associated to initial algae cellulose depolymerisation and to the evaporation of glycerol, and the third stage around 310 °C is related to cellulose depolymerisation and SPI decomposition [53,54]. The TGA curves showed that algae cellulose-containing SPI membranes have suitable thermal stability to be used as separator for batteries [55].

A battery separator should be mechanically stable to cope with different forces (inside and outside batteries) during the fabrication and operation of the battery. In this sense, compression and puncture tests, as well as texture profile analysis, were performed for control and algae cellulose-containing membranes to assess their mechanical behavior. As can be seen in Fig. 5c, the characteristic curves of non-plastically deformed samples were obtained, with an elastic response and shape recovery. Moreover, around 7 kg_f was needed for a deformation of 50 % in all samples (Fig. 5d). As for puncture, the maximum force required for the control sample was 6.03 ± 0.21 N; this value increased with Cell content up to 8.67 ± 0.32 N for 50Cell membrane (Table 1). Since the puncture strength of a thin separator should be higher than 3 N [56], cellulose-containing SPI membranes showed excellent values. Additionally, the energy required for puncture increased from 13.03 ± 0.41 mJ for the control membrane to 18.67 ± 0.33 mJ for 50Cell membrane (Table 1), excellent mechanical behavior for membranes to be used as battery separators. Concerning texture profile analysis (TPA), as shown in Table 1, similar force/area results were obtained in the two cycles of TPA, with cohesiveness values around 0.75 for all membranes,

Table 1
Data from puncture and TPA tests for control, 25Cell, 30Cell, 40Cell and 50Cell membranes.

	PUNCTURE		TPA	
	Maximum force (N)	Rupture energy (mJ)	Cohesiveness	Hardness (kg)
Control	6.03±0.21	13.03±0.41	0.75±0.01	2.36±0.15
25Cell	6.21±0.25	13.39±0.17	0.75±0.01	2.33±0.16
30Cell	7.14±0.40	15.19±0.44	0.76±0.01	2.34±0.17
40Cell	8.32±0.31	17.23±0.41	0.75±0.01	2.33±0.19
50Cell	8.67±0.32	18.67±0.33	0.75±0.01	2.34±0.11

indicating a suitable structural strength that prevents the membrane from decomposing into fragments upon force cycling. Additionally, all samples showed hardness values higher than 2.32 kg. These values are in agreement with the results obtained by puncture tests. Therefore, it could be concluded that algae cellulose-containing membranes are resistant to repetitive force cycles.

Considering the results obtained in the thermal, physicochemical, morphological and mechanical characterization, 50Cell membranes were selected to carry out the studies related to the membrane application.

3.3. Uptake behavior, ionic conductivity and Li^+ transference number

Considering the morphology, the physicochemical properties and the excellent mechanical behavior of the 50Cell membrane, this membrane was tested as a separator for LIBs. Fig. 6a shows the uptake process as a function of time for this membrane with the same dimensions used in cathodic half-cells. It is observed that after 1 min, the membrane is filled by the electrolyte with ~500%, due to the high degree of porosity and also to the pore size of this membrane.

After the uptake process, the ionic conductivity was evaluated through impedance spectroscopy, the Nyquist plot for the 50 Cell membrane being shown in Fig. 6b. The Nyquist plot is characterized by a straight line over the frequency range, demonstrating the high ionic conduction process through charge transfer and Li electrode/electrolyte

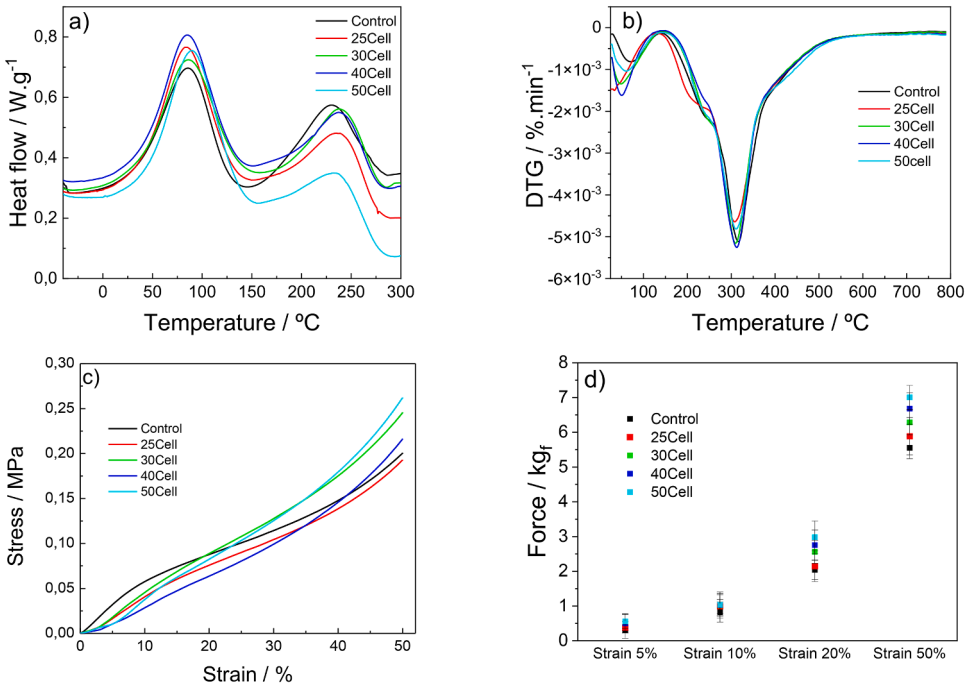

Fig. 5. (a) DSC scans, (b) DTG curves, (c) stress-strain curves and (d) force variation as a function of different strain for control, 25Cell, 30Cell, 40Cell and 50Cell membranes.

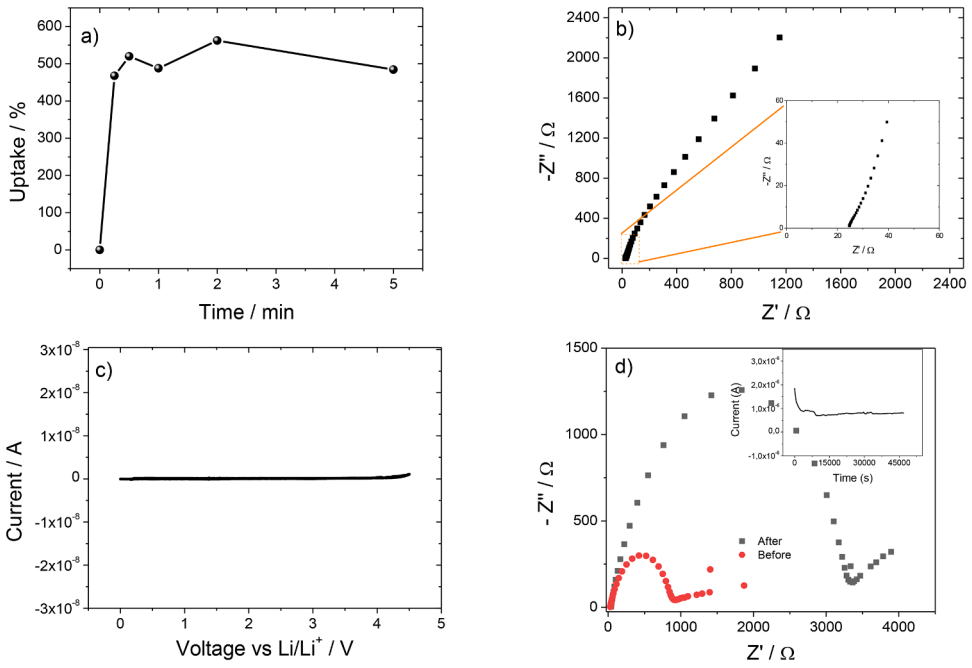

Fig. 6. (a) Electrolyte uptake process, (b) Nyquist plot, (c) cycling voltammetry and (d) DC polarization measurements for the 50Cell membrane.

interface [57]. Eq. 2 was used for calculating the ionic conductivity value of the sample and a value of 5.8 mS.cm^{-1} was obtained for 50 Cell membrane.

For the evaluation of the electrochemical stability of the 50Cell membrane, Fig. 6c shows the cycle voltammogram after the uptake process. In the voltage range from 0 to 5 V, no anodic and cathodic peaks are observed, demonstrating that the membrane is very stable for battery applications.

Finally, an important parameter in separator membranes is the lithium-ion transference number, t_{Li}^{+} which was calculated from the Bruce and Evans method, as shown in Fig. 6d. For this membrane, the t_{Li}^{+} is 0.77, higher than that of commercial separator membranes or carrageenan membranes [15]. This value is due to the excellent compatibility and interaction between the electrolyte solution and the membrane, facilitating ion-pair dissociation and demonstrating that the developed membrane is suitable as LIBs separator.

3.4. Charge/discharge behavior

Considering the high ionic conductivity value and lithium transference number, cathodic half-cells were assembled with the 50Cell membrane to evaluate the charge-discharge behavior at room

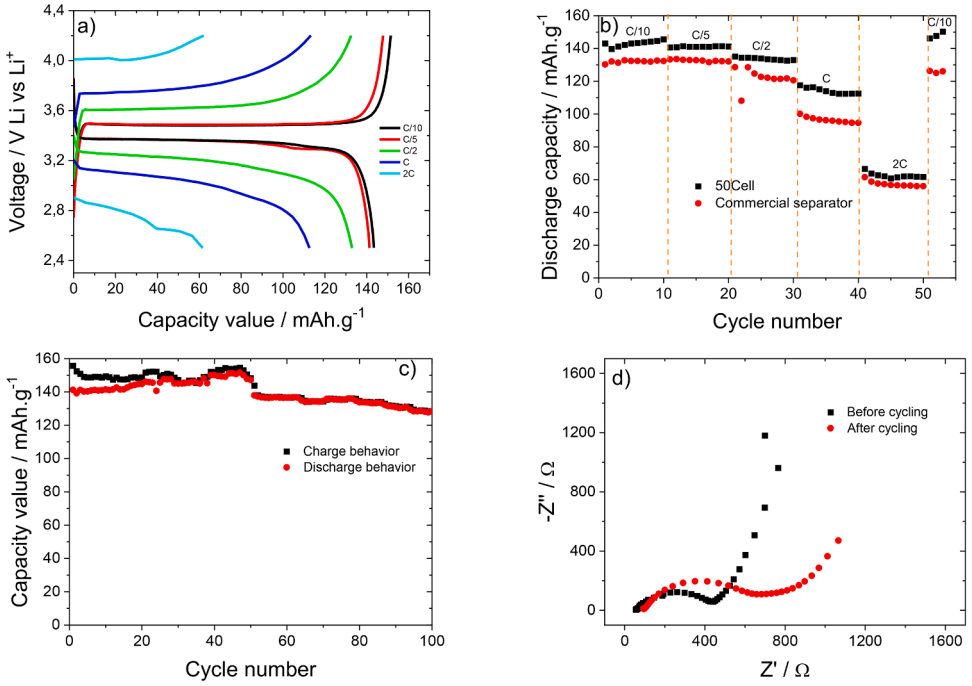

Fig. 7. (a) Charge/discharge profiles at different C-rates, (b) rate performance as a function of the cycle number compared to glass fiber separator, (c) charge and discharge values at C/10-rate for 100 cycles and (d) Nyquist plot before and after cycling for the 50Cell membranes.

temperature and different C-rates. Fig. 7a shows the fifth charge/discharge curve profiles at C/10, C/5, C/2, 1C and 2C-rate. For each C-rate, ten charge/discharge cycles were performed, the curve profile being very similar along the cycle number. Fig. 7a shows the typical redox peaks pair of C-LFP active material, demonstrating the removal of lithium during the charging process and its insertion during discharge process.

The discharge capacity values are 144, 141, 133, 112 and 61 mAh.g^{-1} at C/10, C/5, C/2, 1C and 2C, respectively, demonstrating excellent battery behavior and reversibility. These high discharge capacity values are due to the high ionic conductivity and lithium transference number. It is also observed that the charge and discharge capacity values decrease with the increase of the C-rate due to the ohmic drop polarization process [58]. Furthermore, for all C-rates, the Coulombic efficiency is near ~ 100%, demonstrating the excellent process reversibility.

The cycling behavior of this membrane was compared to that of a commercial glass fiber separator (Whatman GF A) and Fig. 7b shows the rate performance as a function of 10 cycles for each C-rate for both membranes. It is observed that the discharge value is very stable for both membranes as a function of the cycle number for each C-rate and, regardless of the C-rate, the discharge capacity value of the 50Cell membrane is higher compared to the commercial separator due to high ionic conductivity value and lithium transference number (Fig. 7b).

Fig. 7c shows the cycle stability over 100 cycles in the charge and discharge process at C/10 to assess the cyclability of this membrane, showing that the capacity remains practically constant over 100 cycles, demonstrating the good stability of this membrane. Thus, the discharge capacity value before and after 100 cycles are 141 mAh.g^{-1} and 128 mAh.g^{-1}, respectively, which reveals low capacity fade. Also, in the first 20 cycles, a small difference between charge and discharge value is detected due to the solid electrolyte interface (SEI) formation [59].

Fig. 7d shows the Nyquist plot of the cathodic half-cells with the 50Cell membrane before and after cycling. For both Nyquist plots, it is observed a semicircle at high frequency and the straight line at low frequencies. The semicircle represents the interfacial and charge transfer resistances [60] and the straight line describes the Li^+ diffusion process [61]. It is observed that cycling increases the resistance due to the solid electrolyte interface (SEI) layer formation during cycling [60], the resistance being 440 Ω and 700 Ω before and after cycling, respectively.

Table 2 compares the uptake, porosity, ionic conductivity and battery performance (discharge capacity) of the developed membrane with other membranes from different natural polymers reported in the literature.

Table 2 demonstrates that the ionic conductivity value and battery performance of this membrane presents superior behavior in relation to other sustainable membranes reported in the literature. The ionic conductivity value stands out compared to other membranes due to the excellent interaction with the electrolyte solution. In addition, considering the environmental issues and the circular economy, it is shown that LIBs produced from waste materials may lead to excellent behavior successfully addressing the dichotomy between sustainability vs performance. In addition, the porous membrane produced with materials from waste in various food industries, allows these materials to be given a second life with added value while leading to more sustainable batteries. Finally, it is the first time that the membranes based on soy protein have been used as a separator membrane in battery applications allowing to open new sights to natural polymers in the mentioned applicability.

4. Conclusions

Considering the requirements to improve sustainability of materials, processes and applications, as well as circular economy considerations (e.g. valorization of waste products), new separator membranes, based on soy protein and cellulose-containing algae waste, were prepared by freeze-drying for lithium-ion batteries. A porous morphology was obtained, with a degree of porosity around 80–90%, regardless of the algae waste amount, but the average pore size was affected by algae waste content. Through the swelling process, an excellent interaction between electrolyte solution and the membrane was detected, where the vibration bands and thermal properties were independent of the algae waste amount. Further, the membranes are thermally stable up to ~ 150 °C. Mechanical properties were improved by addition of algae waste, demonstrating the excellent interaction between SPI and cellulose; furthermore, the mechanical properties were correlated with the porous morphology. Electrochemical parameters were evaluated for the membranes with the highest algae waste content due to their excellent mechanical properties, and ionic conductivity and lithium transference number values were 5.8 mS.cm^{-1} and 0.77, respectively. Cathodic half-cell with the 50Cell separator membrane showed excellent battery characteristics at different C-rates. Cathodic half-cells prepared with this membrane showed a discharge capacity of 61 mAh.g^{-1} at 2C and 128 mAh.g^{-1} at C/10-rate after 100 cycles, demonstrating outstanding performance. If fact, the obtained results are among the best for battery separator membranes based on natural polymers. Thus, the present work demonstrates that it is possible to obtain sustainable lithium-ion batteries based on waste materials from several industries, giving a second life to these materials and leading to more sustainable batteries.

Table 2
Separator membranes from different natural polymers used in lithium-ion batteries for LFP active material.

Natural polymer	Electrolyte Uptake (%) / Porosity (%)	σ_i (mS·cm^{-1})	Discharge capacity (mAh·g^{-1})	Ref
Carrageenan	700/90	1.34	113@C/5 after 100 cycles	[15]
Silk Fibroin/Silk Sericin	153/86	4.09	86@2C after 100 cycles	[20]
PLLA	345/72	1.6	123@C/5 after 50 cycles	[19]
Silk Fibroin	350/90	2.2	133.3@C/5 after 50 cycles	[62]
O-PHBV/CFO	400/88	5.2	105@C/8 after 100 cycles	[18]
Cellulose	240-280/75	2.1	85@2C after 60 cycles	[16]
Calcium alginate/ cellulose	270/78	1.22	138@C/2 after 50 cycles	[63]
Sodium alginate/ attapulgite	420/68	1.15	123.5@C/2 after 700 cycles	[64]
Agar	-/60	2.5	105@C after 100 cycles	[65]
Chitin	242/54	0.064	105@C/2 after 115 cycles	[66]
Soy protein/ cellulose	500/89	5.8	150@C/10 after 100 cycles	This work

CRediT authorship contribution statement

João P. Serra: Data curation, Formal analysis, Investigation, Writing – original draft. **Jone Uranga:** Data curation, Formal analysis, Investigation, Methodology, Writing – original draft. **Renato Gonçalves:** Methodology, Validation, Formal analysis, Investigation, Writing – original draft, Writing – review & editing. **Carlos M. Costa:** Conceptualization, Investigation, Methodology, Resources, Funding acquisition, Supervision, Validation, Writing – original draft, Writing – review & editing. **Koro de la Caba:** Conceptualization, Investigation, Resources, Funding acquisition, Supervision, Validation, Writing – review & editing. **Pedro Guerrero:** Conceptualization, Investigation, Methodology, Supervision, Validation, Writing – review & editing. **Senentxu Lanceros-Mendez:** Conceptualization, Investigation, Resources, Funding

acquisition, Supervision, Validation, Writing – review & editing.

Declaration of Competing Interest

The authors declare that they have no known competing financial interests or personal relationships that could have appeared to influence the work reported in this paper.

Data availability

Data will be made available on request.

Acknowledgments

The authors thank the Fundação para a Ciência e Tecnologia (FCT) for financial support under the framework of Strategic Funding UIDB/04650/2020, UID/FIS/04650/2020, UID/EEA/04436/2020, and UID/QUI/00686/2020 and under projects MIT-EXPL/TDI/0033/2021, POCI-01-0247-FEDER-046985 and 2022.03931.PTDC funded by national funds through FCT and by the ERDF through the COMPETE2020—Programa Operacional Competitividade e Internacionalização (POCI). The authors also thank the FCT for financial support under Grant 2021.08158.BD (J.P.S.) and FCT investigator contracts CEECIND/00833/2017 (RG) and 2020.04028.CEECIND (C.M.C.). This study forms part of the Advanced Materials program and was supported by MCIN with funding from European Union NextGenerationEU (PRTR-C17.I1) and by The Basque Government under the IKUR program. The authors also thank the project BIDEKO, funded by MCIN/AEI, NextGenerationEU, PRTR. This work was also supported by the (IT1658-22) and Grant PID2021-124294OB-C22 funded by MCI/AEI10.13039/501100011033 and by "ERDF A way of making Europe". J.U. thanks the University of the Basque Country for her fellowship (ESPDOC21/74).

References

[1] Y. Yuan, J. Lu, Demanding energy from carbon, Carbon Energy 1 (2019) 8–12.
[2] M.W. Flinn, Technical change as an escape from resource scarcity: England in the seventeenth and eighteenth centuries. Natural Resources in European History, Routledge, 2021, pp. 139–159.
[3] B.C. Black, Crude Reality: Petroleum in World History, Rowman & Littlefield Publishers, 2020.
[4] E. De Cian, F. Sferra, M. Tavoni, The influence of economic growth, population, and fossil fuel scarcity on energy investments, Clim. Change 136 (2016) 39–55.
[5] A. Olabi, M.A. Abdelkareem, Renewable energy and climate change, Renew. Sustain. Energy Rev. 158 (2022), 112111.
[6] H. Zsiborács, N.H. Baranyai, A. Vincze, L. Zentkó, Z. Birkner, K. Máté, G. Pintér, Intermittent renewable energy sources: the role of energy storage in the european power system of 2040, Electronics 8 (2019) 729.
[7] L. da Silva Lima, M. Quartier, A. Buchmayr, D. Sanjuan-Delmás, H. Laget, D. Corbisier, J. Mertens, J. Dewulf, Life cycle assessment of lithium-ion batteries and vanadium redox flow batteries-based renewable energy storage systems, Sustain. Energy Technol. Assess. 46 (2021), 101286.
[8] T. Chen, Y. Jin, H. Lv, A. Yang, M. Liu, B. Chen, Y. Xie, Q. Chen, Applications of lithium-ion batteries in grid-scale energy storage systems, Trans. Tianjin Univ. 26 (2020) 208–217.
[9] C.M. Costa, S. Lanceros-Mendez, Recent advances on battery separators based on poly (vinylidene fluoride) and its copolymers for lithium-ion battery applications, Curr. Opin. Electrochem. 29 (2021), 100752.
[10] R. Gonçalves, D. Miranda, T. Marques-Almeida, M. Silva, V.F. Cardoso, A. Almeida, C. Costa, S. Lanceros-Méndez, Patterned separator membranes with pillar surface microstructures for improved battery performance, J. Colloid Interface Sci. 596 (2021) 158–172.
[11] R. Gonçalves, D. Miranda, A. Almeida, M.M. Silva, J.M. Meseguer-Dueñas, J. G. Ribelles, S. Lanceros-Méndez, C. Costa, Solid polymer electrolytes based on lithium bis (trifluoromethanesulfonyl) imide/poly (vinylidene fluoride-co-hexafluoropropylene) for safer rechargeable lithium-ion batteries, Sustain. Mater. Technol. 21 (2019) e00104.
[12] M.M. Titirici, Sustainable batteries—Quo vadis? Adv. Energy Mater. 11 (2021), 2003700.
[13] J.C. Barbosa, R. Gonçalves, C.M. Costa, S. Lanceros-Mendez, Recent advances on materials for lithium-ion batteries, Energies 14 (2021) 3145.
[14] O. Olatunji, Natural Polymers: Industry Techniques and Applications, Springer, 2015.
[15] J.P. Serra, A. Fidalgo-Marijuan, J. Teixeira, L. Hilliou, R. Gonçalves, K. Urtiaga, A. Gutiérrez-Pardo, F. Aguesse, S. Lanceros-Mendez, C.M. Costa, Sustainable lithium-ion battery separator membranes based on carrageenan biopolymer, Adv. Sustain. Syst. 6 (2022), 2200279.
[16] R. Goncalves, E. Lizundia, M.M. Silva, C.M. Costa, S. Lanceros-Méndez, Mesoporous cellulose nanocrystal membranes as battery separators for environmentally safer lithium-ion batteries, ACS Appl. Energy Mater. 2 (2019) 3749–3761.
[17] V. Deerattrakul, P. Sakulaue, A. Bunpheng, W. Kraithong, A. Pengsawang, P. Chakthranont, P. Iamprasertkun, V. Itthibenchapong, Introducing hydrophilic cellulose nanofiber as a bio-separator for "water-in-salt" based energy storage devices, Electrochim. Acta 453 (2023), 142355.
[18] J.C. Barbosa, D.M. Correia, A. Fidalgo-Marijuan, R. Gonçalves, M. Fernandes, V. de Zea Bermudez, M.M. Silva, S. Lanceros-Mendez, C.M. Costa, Sustainable lithium-ion battery separators based on poly (3-hydroxybutyrate-co-hydroxyvalerate) pristine and composite electrospun membranes, Energy Technol. 10 (2022), 2100761.
[19] J. Barbosa, A. Reizabal, D. Correia, A. Fidalgo-Marijuan, R. Gonçalves, M. Silva, S. Lanceros-Mendez, C. Costa, Lithium-ion battery separator membranes based on poly (L-lactic acid) biopolymer, Mater. Today Energy 18 (2020), 100494.
[20] A. Reizabal, A. Fidalgo-Marijuan, R. Gonçalves, A. Gutiérrez-Pardo, F. Aguesse, L. Pérez-Álvarez, J. Vilas-Vilela, C. Costa, S. Lanceros-Mendez, Silk fibroin and sericin polymer blends for sustainable battery separators, J. Colloid Interface Sci. 611 (2022) 366–376.
[21] Q. Li, Y. Liu, L. Yang, Y. Wang, Y. Liu, Y. Chen, X. Guo, Z. Wu, B. Zhong, N, O co-doped chlorella-based biomass carbon modified separator for lithium-sulfur battery with high capacity and long cycle performance, J. Colloid Interface Sci. 585 (2021) 43–50.
[22] E. Lizundia, C.M. Costa, R. Alves, S. Lanceros-Méndez, Cellulose and its derivatives for lithium ion battery separators: a review on the processing methods and properties, Carbohydr. Polym. Technol. Appl. 1 (2020), 100001.
[23] D. Lv, J. Chai, P. Wang, L. Zhu, C. Liu, S. Nie, B. Li, G. Cui, Pure cellulose lithium-ion battery separator with tunable pore size and improved working stability by cellulose nanofibrils, Carbohydr. Polym. 251 (2021), 116975.
[24] Z. Du, Y. Su, Y. Qu, L. Zhao, X. Jia, Y. Mo, F. Yu, J. Du, Y. Chen, A mechanically robust, biodegradable and high performance cellulose gel membrane as gel polymer electrolyte of lithium-ion battery, Electrochim. Acta 299 (2019) 19–26.
[25] E. Zanchetta, E. Damergi, B. Patel, T. Borgmeyer, H. Pick, A. Pulgarin, C. Ludwig, Algal cellulose, production and potential use in plastics: challenges and opportunities, Algal Res. 56 (2021), 102288.
[26] M. Martínez-Sanz, V. Cebrián-Lloret, J. Mazarro-Ruiz, A. López-Rubio, Improved performance of less purified cellulosic films obtained from agar waste biomass, Carbohydr. Polym. 233 (2020), 115887.
[27] H. Tian, G. Guo, X. Fu, Y. Yao, L. Yuan, A. Xiang, Fabrication, properties and applications of soy-protein-based materials: a review, Int. J. Biol. Macromol. 120 (2018) 475–490.
[28] R.R. Koshy, S.K. Mary, S. Thomas, L.A. Pothan, Environment friendly green composites based on soy protein isolate–a review, Food Hydrocoll. 50 (2015) 174–192.
[29] D.Y. Xie, D. Qian, F. Song, X.L. Wang, Y.Z. Wang, A fully biobased encapsulant constructed of soy protein and cellulose nanocrystals for flexible electromechanical sensing, ACS Sustain. Chem. Eng. 5 (2017) 7063–7070.
[30] J. Liu, D. Su, J. Yao, Y. Huang, Z. Shao, X. Chen, Soy protein-based polyethylenimine hydrogel and its high selectivity for copper ion removal in wastewater treatment, J. Mater. Chem. A 5 (2017) 4163–4171.
[31] F. Li, T. Liu, W. Gu, Q. Gao, J. Li, S.Q. Shi, Bioinspired super-tough and multifunctional soy protein-based material via a facile approach, Chem. Eng. J. 405 (2021), 126700.
[32] L. Cai, Y. Li, X. Lin, H. Chen, Q. Gao, J. Li, High-performance adhesives formulated from soy protein isolate and bio-based material hybrid for plywood production, J. Clean. Prod. 353 (2022), 131587.
[33] C. Jin, J. Nai, O. Sheng, H. Yuan, W. Zhang, X. Tao, X.W. Lou, Biomass-based materials for green lithium secondary batteries, Energy Environ. Sci. 14 (2021) 1326–1379.
[34] P.G. Bruce, J. Evans, C.A. Vincent, Conductivity and transference number measurements on polymer electrolytes, Solid State Ion. 28-30 (1988) 918–922.
[35] R. Gonçalves, P. Dias, L. Hilliou, P. Costa, M.M. Silva, C.M. Costa, S. Corona-Galván, S. Lanceros-Méndez, Optimized printed cathode electrodes for high performance batteries, Energy Technol. 9 (2021), 2000805.
[36] L.H. Luo, X.M. Wang, Y.F. Zhang, Y.M. Liu, P.R. Chang, Y. Wang, Y. Chen, Physical properties and biocompatibility of cellulose/soy protein isolate membranes coagulated from acetic aqueous solution, J. Biomater. Sci. Polym. Ed. 19 (2008) 479–496.
[37] Z. Li, W. Wang, X. Liang, J. Wang, Y. Xu, W. Li, Fiber swelling to improve cycle performance of paper-based separator for lithium-ion batteries application, J. Energy Chem. 79 (2023) 92–100.
[38] W. Luo, S. Cheng, M. Wu, X. Zhang, D. Yang, X. Rui, A review of advanced separators for rechargeable batteries, J. Power Sources 509 (2021), 230372.
[39] C.F.J. Francis, I.L. Kyratzis, A.S. Best, Lithium-ion battery separators for ionic-liquid electrolytes: a review, Adv. Mater. 32 (2020), 1904205.
[40] J. Jang, J. Oh, H. Jeong, W. Kang, C. Jo, A review of functional separators for lithium metal battery applications, Materials 13 (2020) 4625.
[41] A. Gören, C.M. Costa, M.N. Tamaño Machiavello, D. Cíntora-Juárez, J. Nunes-Pereira, J.L. Tirado, M.M. Silva, J.L. Gomez Ribelles, S. Lanceros-Méndez, Effect of the degree of porosity on the performance of poly(vinylidene fluoride-

trifluoroethylene)/poly(ethylene oxide) blend membranes for lithium-ion battery separators, Solid State Ion. 280 (2015) 1–9.
[42] E. Ansarifar, F. Shahidi, M. Mohebbi, N. Ramezanian, A. Koocheki, A. Mohamadian, Optimization of limonene microencapsulation based on native and fibril soy protein isolate by VIKOR method, LWT 115 (2019), 107884.
[43] L. Zhang, F. Zhang, Y. Fang, S. Wang, Alginate-shelled SPI nanoparticle for encapsulation of resveratrol with enhanced colloidal and chemical stability, Food Hydrocoll. 90 (2019) 313–320.
[44] X. Liu, C.M.G.C. Renard, S. Bureau, C.L. Bourvellec, Revisiting the contribution of ATR-FTIR spectroscopy to characterize plant cell wall polysaccharides, Carbohydr. Polym. 262 (2021), 117935.
[45] C. Trilokesh, K.B. Uppuluri, Isolation and characterization of cellulose nanocrystals from jackfruit peel, Sci. Rep. 9 (2019) 16709.
[46] J. Uranga, M.G. Llamas, Z. Agirrezabala, M.T. Dueñas, O. Etxebeste, P. Guerrero, K. de la Caba, Compression molded soy protein films with exopolysaccharides produced by cider lactic acid bacteria, Polymers 12 (2020) 2106.
[47] A.F. Tarchoun, D. Trache, T.M. Klapötke, Microcrystalline cellulose from posidonia oceanica brown algae: extraction and characterization, Int. J. Biol. Macromol. 138 (2019) 837–845.
[48] I. Chakraborty, S. Rongpipi, I. Govindaraju, R. Bhaskar, S.S. Mal, E.W. Gomez, E. D. Gomez, R.D. Kalita, Y. Nath, N. Mazumder, An insight into microscopy and analytical techniques for morphological, structural, chemical, and thermal characterization of cellulose, Microsc. Res. Tech. 85 (2022) 1990–2015.
[49] P. Dorishetty, R. Balu, A. Sreekumar, L. de Campo, J.P. Mata, N.R. Choudhury, N. K. Dutta, Robust and tunable hybrid hydrogels from photo-cross-linked soy protein isolate and regenerated silk fibroin, ACS Sustain. Chem. Eng. 7 (2019) 9257–9271.
[50] M.H. Parekh, S. Oka, J. Lutkenhaus, V.G. Pol, Critical-point-dried, porous, and safer aramid nanofiber separator for high-performance durable lithium-ion batteries, ACS Appl. Mater. Interfaces 14 (2022) 29176–29187.
[51] H. Fu, J. Li, X. Yang, M.S. Swallah, H. Gong, L. Ji, X. Meng, B. Lyu, H. Yu, The heated-induced gelation of soy protein isolate at subunit level: Exploring the impacts of α and α′ subunits on SPI gelation based on natural hybrid breeding varieties, Food Hydrocoll. 134 (2023), 108008.
[52] L. Zheng, J.M. Regenstein, L. Zhou, Z. Wang, Soy protein isolates: A review of their composition, aggregation, and gelation, Compr. Rev. Food Sci. Food Saf. 21 (2022) 1940–1957.
[53] G. Pinheiro Bruni, J.P. de Oliveira, L.G. Gómez-Mascaraque, M.J. Fabra, V. Guimarães Martins, E.D.R. Zavareze, A. López-Rubio, Electrospun β-carotene–loaded SPI:PVA fiber mats produced by emulsion-electrospinning as bioactive coatings for food packaging, Food Pack. Shelf Life 23 (2020), 100426.
[54] L. Szcześniak, A. Rachocki, J. Tritt-Goc, Glass transition temperature and thermal decomposition of cellulose powder, Cellulose 15 (2008) 445–451.
[55] D. Parikh, T. Christensen, C.T. Hsieh, J. Li, Elucidation of separator effect on energy density of Li-ion batteries, J. Electrochem. Soc. 166 (2019) A3377–A3383.
[56] Z. Lu, F. Sui, Y.E. Miao, G. Liu, C. Li, W. Dong, J. Cui, T. Liu, J. Wu, C. Yang, Polyimide separators for rechargeable batteries, J. Energy Chem. 58 (2021) 170–197.
[57] J.C. Barbosa, R. Gonçalves, A. Valverde, P.M. Martins, V.I. Petrenko, M. Márton, A. Fidalgo-Marijuan, R. Fernández de Luis, C.M. Costa, S. Lanceros-Méndez, Metal organic framework modified poly(vinylidene fluoride-co-hexafluoropropylene) separator membranes to improve lithium-ion battery capacity fading, Chem. Eng. J. 443 (2022), 136329.
[58] A. Gören, J. Mendes, H.M. Rodrigues, R.E. Sousa, J. Oliveira, L. Hilliou, C.M. Costa, M.M. Silva, S. Lanceros-Méndez, High performance screen-printed electrodes prepared by a green solvent approach for lithium-ion batteries, J. Power Sources 334 (2016) 65–77.
[59] Y. Zhang, N. Du, D. Yang, Designing superior solid electrolyte interfaces on silicon anodes for high-performance lithium-ion batteries, Nanoscale 11 (2019) 19086–19104.
[60] J. Guo, A. Sun, X. Chen, C. Wang, A. Manivannan, Cyclability study of silicon–carbon composite anodes for lithium-ion batteries using electrochemical impedance spectroscopy, Electrochim. Acta 56 (2011) 3981–3987.
[61] J. Huang, Diffusion impedance of electroactive materials, electrolytic solutions and porous electrodes: Warburg impedance and beyond, Electrochim. Acta 281 (2018) 170–188.
[62] A. Reizabal, R. Gonçalves, A. Fidalgo-Marijuan, C. Costa, L. Pérez, J.L. Vilas, S. Lanceros-Mendez, Tailoring silk fibroin separator membranes pore size for improving performance of lithium ion batteries, J. Membr. Sci. 598 (2020), 117678.
[63] L. Tan, Z. Li, R. Shi, F. Quan, B. Wang, X. Ma, Q. Ji, X. Tian, Y. Xia, Preparation and properties of an alginate-based fiber separator for lithium-ion batteries, ACS Appl. Mater. Interfaces 12 (2020) 38175–38182.
[64] Q. Song, A. Li, L. Shi, C. Qian, T.G. Feric, Y. Fu, H. Zhang, Z. Li, P. Wang, Z. Li, Thermally stable, nano-porous and eco-friendly sodium alginate/attapulgite separator for lithium-ion batteries, Energy Storage Mater. 22 (2019) 48–56.
[65] M. Shin, W.J. Song, J.G. Han, C. Hwang, S. Lee, S. Yoo, S. Park, H.K. Song, S. Yoo, N.S. Choi, Metamorphosis of seaweeds into multitalented materials for energy storage applications, Adv. Energy Mater. 9 (2019), 1900570.
[66] T.W. Zhang, B. Shen, H.B. Yao, T. Ma, L.L. Lu, F. Zhou, S.H. Yu, Prawn shell derived chitin nanofiber membranes as advanced sustainable separators for Li/Na-ion batteries, Nano Lett. 17 (2017) 4894–4901.